On a modified arrested topographic wave in Fram Strait

P. Schlichtholz
Institute of Oceanology, Polish Academy of Sciences, Sopot, Poland

Received 16 January 2001; revised 8 March 2002; accepted 15 May 2002; published 13 November 2002.

[1] The bottom geostrophic flow in Fram Strait is explained in terms of a modified arrested topographic wave model. The model is based on a combination of the vorticity balance between the topographic vortex stretching and the bottom Ekman pumping due to liner friction with a relation between the bottom flow and the bottom pressure gradient over a sloping bottom. Such a combination emphasizes a dynamical relevance of along-isobath density variations at the bottom. Using an inverse solution based on the hydrographic data from the MIZEX 84 experiment, it is shown that the along-isobath bottom density variations should be dynamically important, for example, in the East Greenland Current. A relatively high correlation between an along-isobath distribution of the bottom geostrophic flow and the bottom density is reported for that current. The density variations identified in the data should be able to drive a bottom geostrophic flow with a magnitude consistent with the inverse solution and observations. *INDEX TERMS:* 4203 Oceanography: General: Analytical modeling; 4207 Oceanography: General: Arctic and Antarctic oceanography; 4211 Oceanography: General: Benthic boundary layers; 4512 Oceanography: Physical: Currents; 4532 Oceanography: Physical: General circulation; *KEYWORDS:* Fram Strait, East Greenland Current, bottom geostrophic flow, arrested topographic wave, bottom density variations, bottom friction

Citation: Schlichtholz, P., On a modified arrested topographic wave in Fram Strait, *J. Geophys. Res.*, *107*(C11), 3189, doi:10.1029/2001JC000799, 2002.

1. Introduction

[2] The linear, frictionless local vorticity equation and one of its vertically integrated versions, the Sverdrup balance, are milestones in the ocean circulation theory [*Pedlosky*, 1996] and the ocean circulation inverse problem [*Wunsch*, 1996]. The Sverdrup balance is between the vorticity imparted by the wind stress curl and the vorticity due to the vertically integrated flow along the gradient of the planetary vorticity (β effect). The balance can hold in the ocean outside the intense western boundary currents and away from the equator. No allowance is made in the Sverdrup balance for influence of bottom topography on the vorticity balance. This is perhaps not a serious problem for a general circulation on timescales of decades or longer. For instance, *Anderson and Killworth*'s [1977] linear spin-up theory, based on a two-layer model with bottom topography, suggests that the Sverdrup balance can be achieved in the ocean interior approximately after the time taken by the baroclinic Rossby wave excited by the wind stress to cross the ocean from east to west. On a seasonal or interannual timescale, bottom topography is likely to influence the barotropic vorticity balance through the topographic β effect. In particular, the seasonal response of the ocean to seasonal variations of wind forcing may be essentially barotropic and tend to establish (away from the western boundary) a topographic Sverdrup balance, as shown, for example, by *Anderson and Corry* [1985] using a two-layer model for the North Atlantic. That balance can hold even in a homogeneous ocean. In a nonhomogeneous ocean it can be further modified by a particular density distribution with regard to bottom topography as discussed, for example, by *Sakamoto and Yamagata* [1996] for a case relevant for the North Pacific.

[3] In particular areas of the ocean, none of the two terms contributing to the classical (flat-bottomed) Sverdrup balance may enter the barotropic vorticity balance. This may easily happen, for example, in the Nordic Seas where over most of the area the topographic β effect should dominate the planetary β effect (large variations in topography and high latitude), and where a considerable weakening of wind forcing occurs in summer [*Jónsson*, 1991]. If neither the advection of planetary vorticity nor wind forcing can compete in the vorticity balance with the topographic vortex stretching, then some friction should come into play (inertial terms assumed negligible). Such a possibility was considered, for example, in a recent inverse modeling study by *Schlichtholz and Houssais* [1999a], hereafter referred to as SH. In SH, the hydrographic data from the MIZEX 84 experiment were inverted for a geostrophic flow in summer in the northern part of the Nordic Seas, in Fram Strait. The strait lies between Greenland and Spitsbergen and is the deepest link between the Arctic Ocean and the rest of the world's ocean (Figure 1). The model in SH was constrained with a steady state, linear vertically integrated vorticity balance which included wind forcing, the planetary and topographic effects as well as bottom friction approximated by a linear

0148-0227/02/2001JC000799$09.00

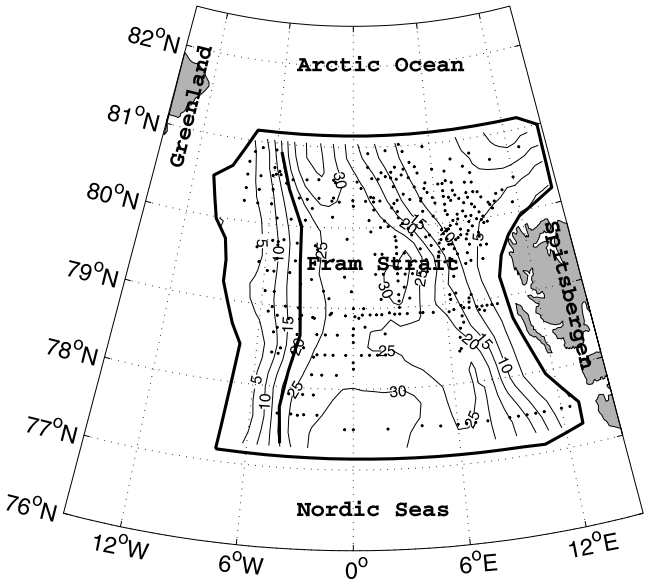

Figure 1. Bottom topography in Fram Strait (in 10^2 m) and the distribution of the hydrographic stations from the MIZEX 84 experiment used in the inverse study by SH. The bold lines show the domain of the inverse model and a section along the EGS, which is of a particular interest for the present study.

drag law. An a posteriori check of the model solutions revealed that the leading vorticity balance in the area is just between the topographic vortex stretching and the curl of the bottom stress, both depending on the bottom geostrophic flow. A considerable bottom flow was obtained in the inverse solutions especially in the western part of the strait, over the East Greenland Slope (EGS).

[4] The vorticity balance between the topographic vortex stretching and the curl of the bottom stress was previously of much interest, for example, in theories of the mean shelf circulation. It forms a basis of the so-called ATW (Arrested Topographic Wave) model, a prototype of which was constructed by *Csanady* [1978]. Various extensions of the model have been proposed. One of them was used by *Shaw and Csanady* [1983] as a dynamical component of their model of self-advection of density perturbations. The dynamics considered by Shaw and Csanady, which can be referred to as the modified ATW (MATW), emphasizes the role of the along-isobath density variations at the ocean bottom. These variations should drive an along-isobath component of the bottom geostrophic velocity.

[5] The present study aims to answer the question whether the bottom geostrophic flow in Fram Strait is likely to be controlled by the bottom density variations. First, the geostrophic dynamics with bottom friction and topography, common for the inverse model and the MATW model, are introduced in section 2. Then the inverse approach and one of the solutions from SH are shortly analyzed in section 3. Next, in section 4, a MATW model similar to that of *Shaw and Csanady* [1983] is constructed. Then, in section 5, the inverse solution is discussed in terms of the MATW model. To focus one's attention, the flow in the East Greenland Current (EGC) over the 2000 m isobath (Figure 1) is considered in more detail. The section is divided into two parts. First, the bottom flow in the EGC is interpreted as a MATW. Next, the MATW model is related to other concepts of exchange between the Arctic Ocean and the Nordic Seas through Fram Strait. A conclusion follows in section 6.

2. Geostrophic Dynamics With Topography and Bottom Friction

[6] Spatial variations of pressure, p, in a "large-scale" flow in the ocean are assumed to be related to the horizontal velocity vector, $\mathbf{u} = (u,v)$, and the seawater density, ρ, through the geostrophic and hydrostatic relations,

$$f\hat{\mathbf{z}} \times \mathbf{u} = -\frac{1}{\rho_0}\nabla p, \tag{1}$$

$$0 = -\frac{\partial p}{\partial z} - g\rho, \tag{2}$$

where $f = 2\Omega\sin\varphi$ is the Coriolis parameter for earth rotation rate Ω ($\approx 7.29 \times 10^{-5}$ s^{-1}), ρ_0 (≈ 1027 kg m^{-3}) is a reference density, g (≈ 9.8 m s^{-2}) is the mean acceleration of gravity, and z is a coordinate in the local vertical direction, in which $\hat{\mathbf{z}}$ is a unit vector. In spherical coordinates (λ, φ, z), where λ and φ are longitude and latitude, the horizontal gradient operator, ∇, is

$$\nabla = \frac{1}{a}\left(\frac{1}{\cos\varphi}\frac{\partial}{\partial\lambda}, \frac{\partial}{\partial\varphi}\right), \tag{3}$$

where a ($\approx 6.37 \times 10^6$ m) is the mean earth's radius.

[7] A known "large-scale" density distribution determines the vertical shear of the geostrophic velocity through the so-called "thermal wind" relation obtained by combining (1) and (2). Integrating the "thermal wind" relation from the ocean bottom, $z = -H$, to a depth z yields the absolute geostrophic velocity as a function of the horizontal density gradients in the ocean interior and the geostrophic velocity at the bottom, $\mathbf{u}_b$,

$$\mathbf{u}(\lambda,\varphi,z) = \mathbf{u}_b(\lambda,\varphi) - \hat{\mathbf{z}} \times \frac{g}{f\rho_0}\int_{-H}^{z} \nabla\rho dz. \tag{4}$$

The bottom geostrophic velocity is a function of pressure at $z = -H$, p_b, and also of the density at the bottom, ρ_b, if the bottom is not flat,

$$\begin{aligned}\mathbf{u}_b &= -\frac{1}{f\rho_0}(\nabla p)_b \times \hat{\mathbf{z}} \\ &= -\frac{1}{f\rho_0}\nabla\rho_b \times \hat{\mathbf{z}} + \frac{g\rho_b}{f\rho_0}\nabla H \times \hat{\mathbf{z}}.\end{aligned} \tag{5}$$

[8] The horizontal divergence of the horizontal velocity is, by the continuity equation, compensated by the vertical gradient of the vertical component of the velocity vector, w,

$$\nabla \cdot \mathbf{u} + \frac{\partial w}{\partial z} = 0. \tag{6}$$

Taking the curl of the geostrophic relation (1) and using (6) yields the vorticity balance between the advection of the

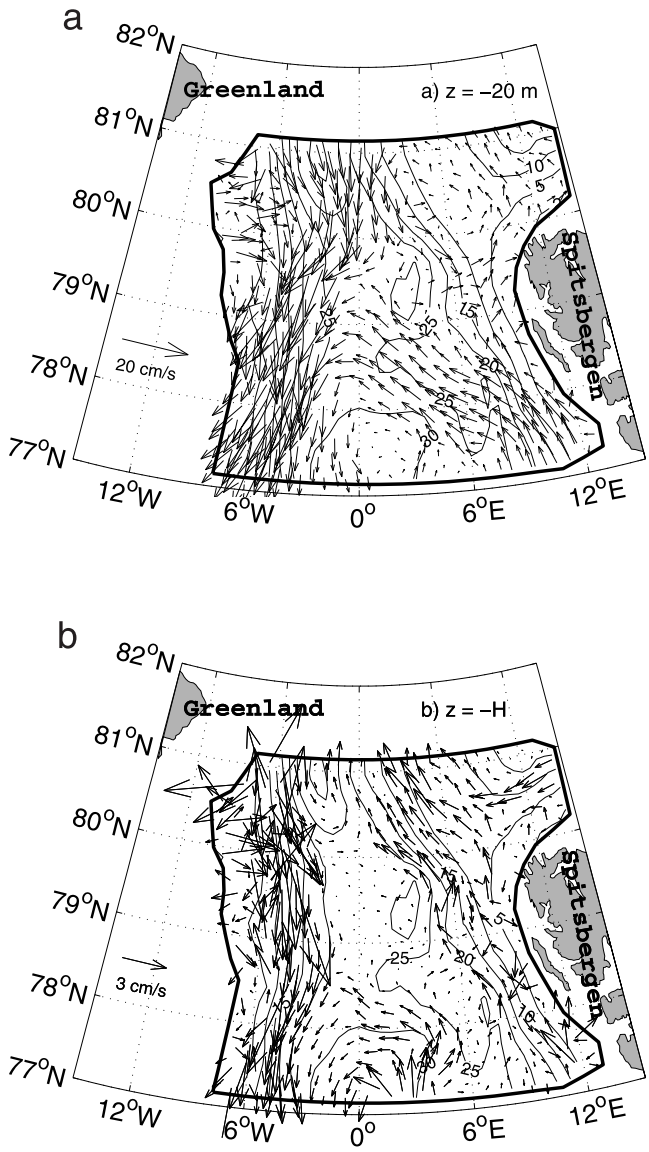

Figure 2. Horizontal distribution of the geostrophic velocity (in cm s^{-1}) obtained from the inverse solution: (a) at $z = -20$ m and (b) at the ocean bottom (note different velocity scaling).

planetary vorticity and the vortex stretching in the planetary vorticity field,

$$\beta v = f\frac{\partial w}{\partial z}, \tag{7}$$

where β is the northward gradient of the Coriolis parameter.

[9] Integrating (7) throughout the water column in a flat-bottomed ocean yields the Sverdrup balance,

$$\beta\int_{-H}^{0} v dz - f w_s = 0, \tag{8}$$

where w_s is the Ekman pumping velocity related to the distribution of the wind stress at the ocean surface, τ_s,

$$w_s = \hat{\mathbf{z}}\cdot\nabla\times\left(\frac{\boldsymbol{\tau}_s}{f\rho_0}\right). \tag{9}$$

For a validity of (8), the vertical velocity at the ocean bottom, w_b, must vanish. In the presence of bottom topography, and when friction is important at the ocean bottom, the appropriate boundary condition is

$$w_b = w_t + w_f = -\mathbf{u}_b\cdot\nabla H + \hat{\mathbf{z}}\cdot\nabla\times\left(\frac{\boldsymbol{\tau}_b}{f\rho_0}\right). \tag{10}$$

The vertical velocity in equation (10) is the sum of the topographic vortex-stretching velocity, w_t, resulting from the condition that the velocity normal to the bottom is zero, and the Ekman pumping velocity, w_f, due to bottom friction, $\boldsymbol{\tau}_b$.

[10] Both equations (9) and (10) are boundary conditions for the interior flow and, strictly, should be applied at the bottom of the surface Ekman layer and the top of the bottom Ekman layer, respectively. In practice, the thickness of the Ekman layers is assumed negligible compared to the ocean depth. Vertically integrating equation (7) with the boundary conditions (9) and (10) leads to the following vorticity balance:

$$\beta\int_{-H}^{0} v dz - f w_s = -f\left(w_t + w_f\right). \tag{11}$$

[11] The wind stress may be assumed known but the bottom friction term in (11) depends on flow variables. A simple parameterization of w_f is by a linear drag law,

$$\boldsymbol{\tau}_b = r\rho_0\mathbf{u}_b, \tag{12}$$

where r is a constant friction coefficient with a unit of velocity.

3. Inverse Modeling: Approach and Main Results

[12] In SH it was assumed that the vorticity balance equation (11) holds approximately in Fram Strait. Using equations (1), (10), (12), and (5), the balance can be written in terms of pressure and wind forcing. When allowing for a residual, R, the balance becomes

$$\frac{\beta}{\rho_0 f a\cos\varphi}\int_{-H}^{0}\frac{\partial p}{\partial\lambda}dz + \frac{1}{\rho_0}J(H,p_b) + f\nabla\cdot\left(\frac{r}{\rho_0 f^2}(\nabla p)_b\right) - f w_s = R, \tag{13}$$

where J is the Jacobian operator. The vorticity balance equation (13) and the hydrostatic equation (2) were used in SH as dynamic constraints on the pressure field. The density data from the MIZEX 84 hydrographic stations, located as shown in Figure 1, were assumed to be noisy and entered the problem of estimating the flow in an optimization procedure. The functional minimized in SH can be written as

$$\sum_{i=1}^{N}\gamma_i\left[\left(\frac{\partial p}{\partial z}\right)_i + g\rho_i\right]^2 + \gamma_S S + \gamma_R\int\int\int R^2 a^2\cos\varphi d\lambda d\varphi dz = \min, \tag{14}$$

where N is the number of density data, ρ_i, the index i with the vertical pressure gradient means that the gradient is evaluated at the coordinates of ρ_i, γ_i's are local weighting factors associated with the data, S is a roughness norm ensuring a smooth solution, while γ_S and γ_R are global weighting factors associated with the roughness norm and the dynamical

constraint, respectively. To solve equation (14), the original density data plus an objectively analyzed subset of these data were used. The wind data were taken from a meteorological model. The sought for pressure field had an analytical form. It was decomposed into a number of vertical modes and the mode amplitudes were described by piecewise polynomials on a finite element grid. Analytical bottom topography was constructed using the same grid (see SH for details).

[13] Once the pressure is found, the geostropic velocity and the density distribution can be estimated from equations (1) and (2) at any point of the domain shown in Figure 1. As an example, one of the solutions obtained in SH (p_5 according to the symbols therein) will be analyzed below. The solution is consistent with the density data to an error of magnitude provided by an objective analysis. It satisfies the vorticity balance (13), with the domain-averaged residual, $\overline{|R|}$, of the order of 15% of the magnitude of the leading terms. The residual is due to missed dynamics, errors in data and methodological limitations, for example, a fit to analytical functions with a limited number of the degrees of freedom. The solution is also in a satisfactory agreement with a few current meter data obtained in the EGC during the MIZEX 84 experiment and reported by *Manley et al.* [1987] (see SH for details).

[14] The main features of the circulation in Fram Strait are depicted by the geostrophic velocity at a subsurface level ($z = -20$ m) in Figure 2a. (Note that the velocity in this figure corresponds to the geostrophic stream function in Figure 13a in SH. Unfortunately, some figure captions are permuted in SH; the captions of Figures 11, 12, and 13 are placed below Figures 13, 11, and 12, respectively.) On the western side of the strait one can see the EGC flowing southward, while on the eastern side one finds the West Spitsbergen Current flowing northward. Some recirculations between the two currents are present. Although the flow shows a considerable vertical shear, the bottom geostrophic velocity is significant (Figure 2b). The most intense flow is concentrated mainly along the continental slopes, with a maximum speed in the EGC over the EGS. A relatively large magnitude of the bottom velocity is consistent with the leading vorticity balance, which is between the vortex stretching due to the cross-isobath flow and the curl of the bottom stress (Figures 3a and 3b). The two terms are particularly large over the EGS. The planetary vorticity and the surface Ekman pumping terms are about 2 orders of magnitude smaller.

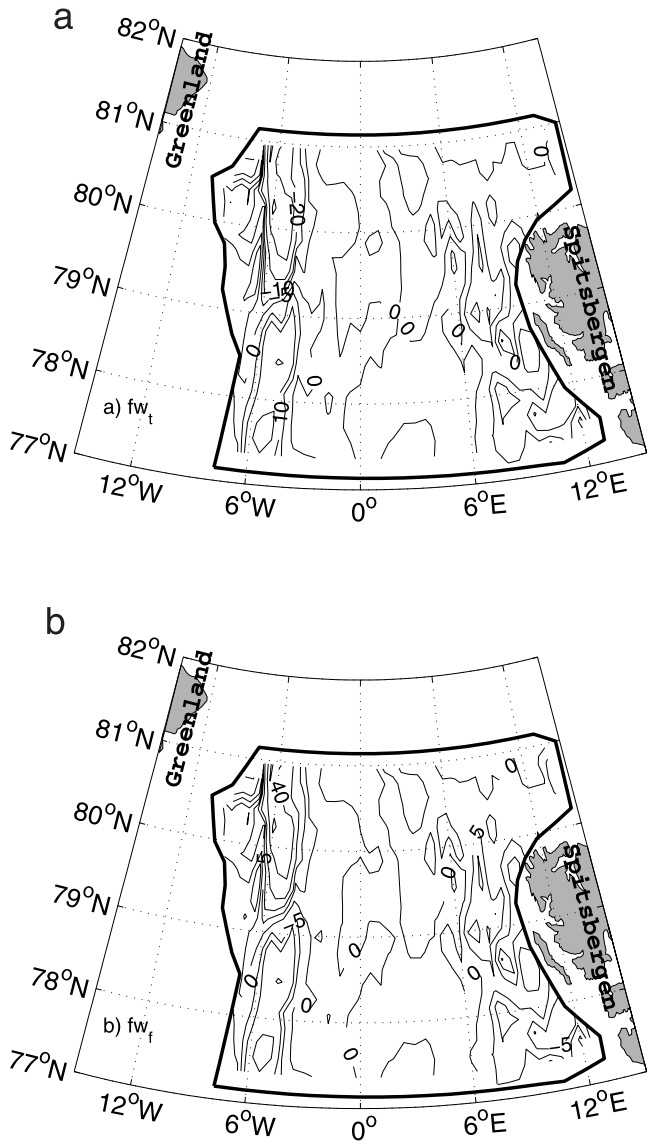

Figure 3. Distribution of the major terms of the vertically integrated vorticity balance equation (11) obtained from the inverse solution: (a) topographic vortex stretching and (b) bottom Ekman pumping. Isocontours are 0, ±5, ±10, ±20, and then every $\pm 20 \times 10^{-9}$ m s^{-2}.

4. Modified Arrested Topographic Wave Model

[15] To interpret the results of the inverse model, let us construct a MATW model. First, neglect the β term and the wind stress term in the vorticity balance equation (11), as suggested by the inverse model. Then, with equation (12) for bottom friction, equation (11) becomes, after division by f,

$$\mathbf{u}_b \cdot \nabla H = r\hat{\mathbf{z}} \cdot \nabla \times \left(\frac{\mathbf{u}_b}{f}\right). \tag{15}$$

Next, consider a flow over a bottom sloping only in the east-west direction so that the ocean depth can be idealized as a function of only longitude. This is a rough approximation, for example, for the EGS in Fram Strait (Figure 1). Furthermore, introduce cross-isobath and along-isobath coordinates, x and y, respectively, defined from a characteristic latitude φ_c as $x = (a \cos \varphi_c)\lambda$ and $y = a(\varphi - \varphi_c)$. Finally, neglect friction in the cross-isobath direction. Equation (15) becomes

$$f_c u_b \left(m_c \frac{dH}{dx}\right) = r\left(m_c \frac{\partial v_b}{\partial x}\right), \tag{16}$$

where $m_c = \cos \varphi_c / \cos \varphi$. A constant value of the Coriolis parameter, f_c, has been assumed in (16) to emphasize the Fram Strait case where $2\Omega \sin \varphi \approx \text{const} = 1.4 \times 10^{-4}$ s^{-1}.

[16] Equation (16) is the vorticity balance of the MATW model, written in spherical coordinates. The balance provides a relation between the cross-isobath flow and the cross-isobath variation of the along-isobath flow. A validity

of that balance requires that the flow be anisotropic. The relevant assumption is

$$\varepsilon_U^2 \equiv \left(\frac{U}{V}\right)^2 = \left(\frac{l}{L}\right)^2 \ll 1, \tag{17}$$

where U and V are the scales of the cross-isobath and along-isobath components of the horizontal velocity, respectively, while l and L are the corresponding length scales. This approximation is indeed justified for the EGC over the EGS (Figure 2b). Moreover, the anisotropy parameter ε_U should be equal to a nondimensional friction parameter, μ_d,

$$\varepsilon_U^2 = \mu_d^2 \equiv \left(\frac{r}{f_c d}\right)^2 \ll 1, \tag{18}$$

where d is a vertical scale of the variation in topography.

[17] An implication of equation (16) is that variations of the bottom density along the isobaths are dynamically relevant. This is shown by an equation for the along-isobath component of the bottom geostrophic velocity derived from equations (16) and (5). We obtain

$$\frac{r}{f_c} m_c \frac{\partial}{\partial x}\left[\left(m_c \frac{dH}{dx}\right)^{-1} m_c \frac{\partial v_b}{\partial x}\right] + m_c \frac{\partial}{\partial y}\left(\frac{v_b}{m_c}\right) = -\frac{g}{f_c \rho_0} m_c \frac{dH}{dx}\frac{\partial \rho_b}{\partial y}. \tag{19}$$

[18] In Cartesian geometry (m_c = 1), and for a constant slope $dH/dx = s = d/l$, (19) becomes,

$$K\frac{\partial^2 v_b}{\partial x^2} + \frac{\partial v_b}{\partial y} = -\kappa \frac{\partial \rho_b}{\partial y}, \tag{20}$$

where $K = \mu_d l$ and $\kappa = gs/f_c\rho_0$. Equation (20), with the right-hand side (RHS) neglected, is analogous to the governing equation (in the sea surface elevation) of the ATW model constructed by *Csanady* [1978]. With the RHS included, equation (20) is similar to the equation for v_b in the model of *Shaw and Csanady* [1983]. A simple interpretation of equation (20) can be made by analogy with a "diffusion" equation [*Csanady*, 1978]. The "diffused" quantity is v_b. The role of time is played by negative y. K is the analog of a diffusion coefficient. The term in the along-isobath gradient of ρ_b is a source term.

[19] Along-isobath variations of ρ_b appearing on the RHS of equation (19) or (20) are indeed present in the MIZEX 84 hydrographic data, as shown by distributions of a bottom density anomaly along the 2000 m isobath over the EGS obtained from inverse solutions (Figure 4). The distributions show that the variations of ρ_b are not merely a response of the model to the applied dynamical constraint, which could force such variations. They are present in the dynamically constrained solution (crosses) and also in the interpolated density field (circles) obtained by solving the nonconstrained version of (14), i.e., with $\gamma_R = 0$.

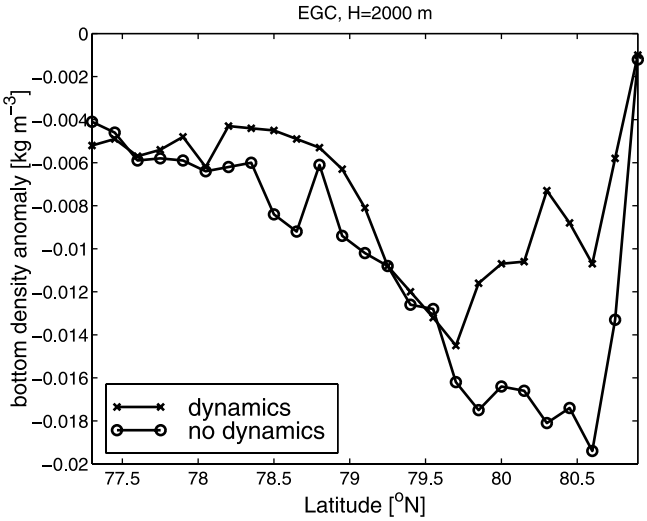

Figure 4. Distributions of the anomaly of the bottom density (in kg m^{-3}) along the isobath H = 2000 m of the EGS in Fram Strait. One distribution is obtained from the inverse solution (crosses) and the other is obtained from the interpolated density field found by solving (14) with γ_R = 0 (circles). The density anomaly is relative to the average of the density at $z = -2000$ m calculated over the entire strait.

5. Discussion

5.1. Bottom Flow in the EGC as a MATW

[20] Equation (20) together with the bottom density distributions in Figure 4 suggest, but not prove, that the along-isobath bottom flow in the EGC is driven by the along-isobath variations of ρ_b. A question arises whether the evidenced density variations are large enough to force a significant bottom flow. The ratio of the time-like and "diffusion" terms in equation (20) scales as the ratio of the anisotropy parameter ε_U and the nondimensional friction parameter μ_d, defined in equations (17) and (18), respectively. Therefore, by construction of the MATW model, the two terms on the left-hand side of equation (20) should have a same magnitude. On the other hand, the magnitude of the source term on the RHS of (20) is not constrained by the model assumptions. Equations leading to equation (20), i.e., the vorticity balance equation (16) and the relation between the bottom geostrophic flow and the gradient of the bottom pressure in equation (5), can be valid even in the extreme case of a homogeneous ocean ($\rho_b = \rho_0$).

[21] The magnitude of parameters μ_d and ε_U can be estimated using the results of the inverse model. With the scale of the bottom depth variation d = 2000 m and the value of the dimensional friction coefficient applied in the model (r = 1 cm s^{-1}), μ_d is about 0.04. A distribution of the components of the bottom geostrophic velocity along the isobath H = 2000 m of the EGS from solution p_5 is shown in Figure 5. The averaged magnitude of v_b (crosses in Figure 5) is about 2.5 cm s^{-1}. Similar values are also obtained from other solutions from SH except for solution p_3 in which $|v_b|$ is too small due to an excessive smoothing of the pressure field (too a large value of γ_S in equation (14)). The current meter measurements of *Foldvik et al.* [1988] suggest that the magnitude of the near-bottom velocity over the EGS at 79°N is indeed O(3 cm s^{-1}). The averaged magnitude of u_b (circles in Figure 5) is about 0.25 cm s^{-1} so that ε_U is about 0.1. The same estimate of ε_U is also obtained using solution p_4 from SH. Compared to other solutions, a common feature of solutions p_4 and p_5 is use of smoother bottom topography in equation (14). The smoothest tropography, shown in Figure 1, was applied for solution p_5. In other solutions,

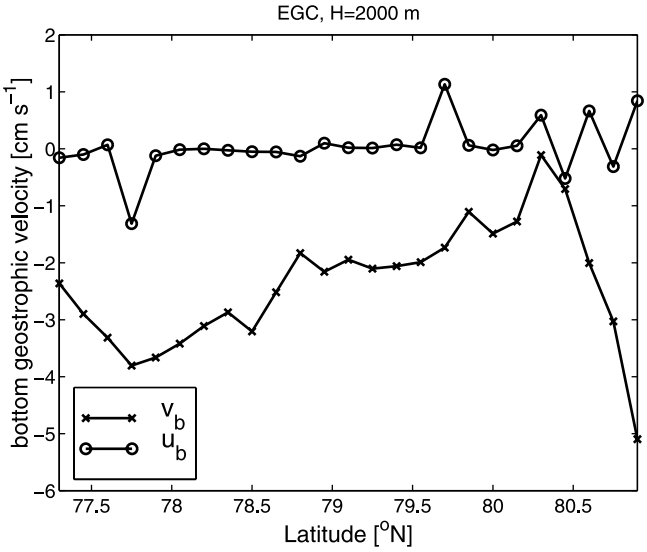

Figure 5. Distribution of the along-isobath (crosses) and cross-isobath (circles) bottom geostrophic velocity (in cm s^{-1}) along the isobath H = 2000 m of the EGS in Fram Strait obtained from the inverse solution. Negative values of v_b and u_b correspond to motion toward the Nordic Seas and upslope motion, respectively.

ε_U is slightly larger (about 0.2) except for the already mentioned unsatisfactory solution p_3 in which it is much larger (about 0.4). With ε_U = O(0.1), the along-isobath length scale should be O(500 km) if l = 50 km is taken for the cross-isobath length scale. Close to this estimate of L is, for example, the distance along the EGS over which an increase of the magnitude of the bottom velocity in the EGC is identified (Figure 5). The increase is present over a distance of about 300 km between, approximately, 80.5°N and 77.5°N. The accordance between ε_U and μ_d is quite good in view of the approximations used in the MATW model, a residual allowed in the inverse solution, errors in approximating the components of the bottom velocity, and the subjective choice of d = 2000 m. Moreover, if only the points satisfying the assumption of a small cross-isobath flow are retained, say those for which $|u_b/v_b| < 0.3$, the estimate of ε_U is about 0.04, and the agreement between ε_U and μ_d becomes perfect.

[22] Of course, the magnitude of μ_d depends on the value of r. The value cited above is larger by one or two orders of magnitude than typical values used in the shelf circulation models [e.g., *Csanady*, 1978]. Trials of solving equation (14) for values of r which are significantly smaller than 1 cm s^{-1} failed. The a posteriori residual of the vorticity balance in these experiments is of the order of the topographic vortex-stretching term. This suggests that the value r = 1 cm s^{-1} might be of a correct order of magnitude for the EGC in Fram Strait. Similar values of r were also considered as plausible by *Schlichtholz and Houssais* [1999b] based on a quite different argument (a plausible estimate of the transport in the EGC obtained from an analytical model). With r = 1 cm s^{-1}, the Ekman layer thickness, estimated as $h_b = r/f_c$, is about 70 m. Even though this estimate of h_b is large, it does not contradict the presence of a geostrophic interior layer over the EGS.

[23] The ratio of the source term to, for example, the time-like term in equation (20) scales as $\kappa\Delta\rho/V$, where $\Delta\rho$ is an estimate of the bottom density variation along the isobaths. According to Figure 4, $\Delta\rho$ is O(0.01 kg m^{-3}) in the EGC. With the bottom slope s = 0.04, the coefficient κ is about 3 m^4 kg^{-1} s^{-1} so that its product with $\Delta\rho$ is O(3 cm s^{-1}). This estimate is in agreement with the scale of the variation of v_b along the EGS from 80.5°N to 77.5°N (Figure 5). Therefore, the source term is of a same magnitude as the other terms in equation (20). However, some details of the density distributions in Figure 4 should be explained. The spectacular increase of ρ_b toward the Arctic Ocean to the north of about 80.5°N, present in both curves, must be an artifact of the model because hydrographic stations over deep isobaths were only available between about 77.5°N and 80.5°N (Figure 1). In addition, not all stations went to the bottom which may explain, for example, the discrepancy between the constrained and interpolated density distributions found to the north of about 79.8°N. The distributions of ρ_b along the same isobath but obtained from other solutions from SH (p_0–p_4) resemble the distribution from the solution analyzed here (p_5). The domain-averaged relative weight given to the agreement with the data in the dynamically constrained solutions was only about 5% of that in the interpolation experiment. Such a large decrease of the weight affected first of all the parts of the model domain in which only a small number of original data were available. From 25 stations in the EGC between the isobaths H = 1500 m and H = 2500 m in which the deepest measurement was from below the level z = −1500 m, only 5 stations were located to the north of 79.8°N. In particular, near-bottom data were lacking in the vicinity of the 2000 m isobath between 79.8°N and 80.5°N, as shown in Figure 6. The figure presents the distribution of a density anomaly at a near-bottom level (z = −1900 m) based on the original data from the stations at which the bottom depth falls between H = 1900 m and H = 2200 m. Although this is not exactly an along-isobath distribution, it demonstrates the general tendency of a southward increase of the near-bottom density in agreement with the interpolated ρ_b.

[24] The simplest representation of the along-isobath variations of ρ_b is by a uniform gradient. Assume that the uniform gradient is equal to $-\Delta\rho/L$ at $y \le 0$, and over the distance l across the isobaths, i.e., for $0 \le x \le l$. Then the source term is constant in equation (20). An analytical solution of a similar equation for the surface elevation in the context of freshwater influx at the shore was studied by *Csanady* [1978]. The author gave, among others, an approximate solution valid at large $(-Ky)^{1/2}$ [see *Csanady*, 1978, equation (30)]. That solution is, in terms of our variable and coefficients,

$$v_b = -\frac{\kappa\Delta\rho}{2KL}\left(4l\pi^{-1/2}(-Ky)^{1/2} - x^2\right). \qquad (21)$$

Because of inherent approximations, equation (21) cannot be used to predict a realistic structure of the along-isobath bottom velocity in the EGC. However, the main features of this flow can be diagnosed from equation (21). For large $-y$, the sign of the analytical flow (negative) is in agreement with the sign of the flow in the EGC. For a given x, the magnitude of the negative flow increases with negative y. At $y = -L$, v_b estimated by equation (21) is from O(1 cm s^{-1}) to O(5 cm s^{-1}), i.e., of a correct magnitude.

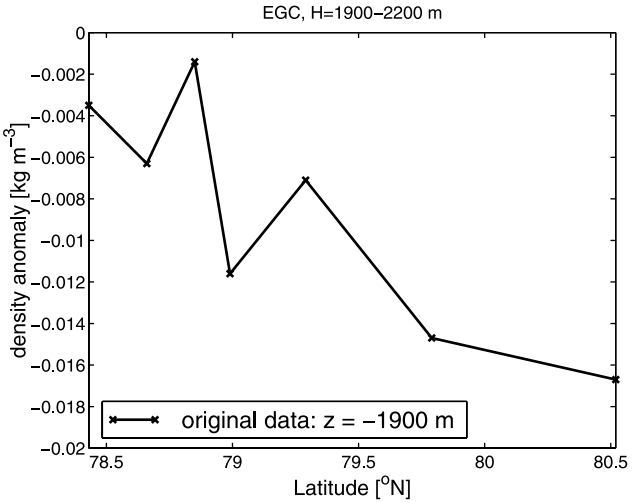

Figure 6. Distribution of the density anomaly at $z = -1900$ m (in kg m^{-3}) along a line following approximately the isobath $H = 2000$ m of the EGS in Fram Strait obtained from the original MIZEX 84 data. The bottom depth at the hydrographic stations from which the data were extracted ranges between $H = 1900$ m and $H = 2200$ m. The density anomaly is relative to the average of the density at $z = -1900$ m calculated over the entire strait.

[25] Equation (20) suggests further that the along-isobath distributions of v_b and ρ_b might be correlated. The correlation coefficient between the crosses in Figure 5 and the crosses in Figure 4 is indeed relatively large (-0.66). The coefficient is even larger (-0.81) if it is calculated using the dynamically constrained distribution of v_b from Figure 5 and the interpolated density distribution (circles in Figure 4). This may be a coincidence in view of the complexity of the variational equation (14), the scarcity and uneven distribution of the original near-bottom data, and an analytical form of the model variables and bottom topography. In another very plausible solution from SH, i.e., p_4, the correlation coefficient between v_b and ρ_b from the solution is the same (-0.67) as between v_b and the interpolated ρ_b. In other solutions, the correlation between v_b and ρ_b is not as good as in p_5 or p_4. Furthermore, if the points for which $|u_b/v_b| < 0.3$ (concentrated mainly in the uncertain northern part) are not included in the calculation of the correlation coefficient, the coefficient becomes large for any solution, ranging from -0.65 to -0.78. The largest coefficient is again for solutions p_5 and p_4, in both cases equal to -0.78, and in both cases equal for either the density from the solution itself or for the interpolated ρ_b. It is worthwhile noting that no explicit relationship between the bottom velocity and the bottom density was assumed in equation (14). Only a weighted agreement between the hydrostatic relation in a three-dimensional domain and the vertically integrated vorticity balance was sought. Therefore, the evidenced high correlation between v_b and ρ_b strengthens the conclusion that the bottom flow in the EGC is a MATW.

5.2. Comparison With Some Earlier Concepts of Exchange Through Fram Strait

[26] The fact that local wind forcing is not a main driving agent for currents in Fram Strait had been known long before the results of the inverse model were published by SH. For instance, in his review of the physical oceanography of Fram Starit, *Hunkins* [1990] quoted earlier studies to argue that the mean geostrophic current beneath the ice in the EGC in the strait is more important for ice motion than the local wind, and pointed out that the ice-free West Spitsbergen Current flows against the wind. On the other hand, the mean wind stress drives a cyclonic gyre to the south of the strait, in the Nordic Seas [*Aagaard*, 1970], and it is responsible for an anticyclonic movement of ice and the upper ocean to the north of the strait, in the Arctic Ocean [*Colony and Thorndike*, 1984]. Therefore, it is possible that the exchange through the strait may be driven by pressure gradients imposed by remote winds. This hypothesis motivated *Hunkins and Whitehead* [1992] to carry out a series of laboratory experiments using a rotating tank with two layers of water having different densities and forced into motion by wind stress applied at the surface of the lighter layer. The geometry of the tank, two semicircular basins divided by a wall with a gap permitting exchange of the lighter water, was intended to represent roughly the Arctic Ocean/Fram Strait/Nordic Seas area. A simplified distribution of wind forcing resembling the real wind field in the area, i.e., a negative wind stress curl over one of the basins (the "Arctic Ocean"), a positive wind stress curl over the other basin (the "Nordic Seas"), and a zero wind stress curl along the gap in the wall ("Fram Strait"), was imposed. The lighter water was found to move into the "Arctic Ocean" which contradicts the observations. This indicated that the exchange through Fram Strait is rather buoyancy-driven than wind-driven.

[27] To emphasize the scenario of a buoyant flow through Fram Strait, *Hunkins and Whitehead* [1992] carried out also "lock exchange" experiments in which water of different densities filled initially an upper part of two basins separated by a gate. In both basins there was a passive deep layer filled with a dense water representing the deep water in the Fram Strait area. The active upper layers represented surface waters in the Arctic Ocean (the lightest water) and in the Nordic Seas (the water of intermediate density). In accordance with observations, narrow boundary currents constrained by rotational effects appeared after the gate was removed. Particularly remarkable was the "East Greenland Current" transporting fluid from the light side to the intermediate side. Before the study of *Hunkins and Whitehead* [1992], laboratory simulations of the EGC were also carried out by *Wadhams et al.* [1979].

[28] Similarly, earlier analytical modeling of exchange through Fram Strait was concentrated on the buoyancy effects. For instance, in a two-layer geostrophic model by *Stigebrandt* [1981], the EGC was considered as the outflowing part of an estuarine-type circulation in the Arctic Ocean. An explanation of the current in terms of a uniform potential vorticity model applied to an inclined frontal system between the lighter (polar) and denser (atlantic) water observed in Fram Strait was provided by *Manley et al.* [1987].

[29] None of the above mentioned laboratory experiments and analytical models made an attempt to incorporate a deep flow in Fram Strait. However, direct velocity measurements indicated that velocities in a deep layer are nonnegligible over the continental slopes on both sides of the strait

[*Aagaard et al.*, 1973; *Foldvik et al.*, 1988]. In the case of the EGC, a barotropic component was evidenced from recordings over both monthly and yearlong periods [*Manley et al.*, 1987; *Foldvik et al.*, 1988]. Even though the near-bottom velocity is smaller than the near-surface velocity, it may contribute considerably to the total transport since the vertical integration reduces the importance of extreme values of the shear flow given by the second term on the RHS of equation (4). The measurements of *Foldvik et al.* [1988] showed that the contributions from the shear and near-bottom flows to the total transport in the EGC are approximately the same. Therefore, the deep flow cannot be neglected in concepts of exchange through Fram Strait. For some time the measurements of *Foldvik et al.* [1988] and *Manley et al.* [1987] were considered evidence for considerable (remote) wind forcing on the basis of an argument that a buoyancy-driven circulation is expected to be essentially baroclinic. However, this interpretation overlooks the important role of bottom topography in ocean dynamics.

[30] The MATW model shows that a buoyancy forcing may be responsible for time mean deep exchange through Fram Strait. Certainly, it explains the presence of the deep flow in summer 1984 when the data supporting the model were collected. A density contrast between the deep layers of the Arctic Ocean and the Nordic Seas, required for validity of the MATW model in Fram Strait, is caused by different scenarios of the deep water formation in these two parts of the Arctic Mediterranean. Already *Aagaard et al.* [1985] considered density differences between the deep water masses of the Arctic Mediterranean as important for the deep outflow from the Arctic Ocean. However, the emphasis in their study was put on the differential compressibility effect for waters with different temperature and salinity characteristics. Effects of a sloping bottom were not considered. On the other hand, several studies emphasized the role of topography as a guiding agent for the flow in Fram Strait without a reference to density variations in a deep layer. In particular, it was speculated that a part of the Sverdrup flow in the Nordic Seas is guided out of the locally wind-driven area by topography to become the West Spitsbergen Current [e.g., *Hunkins*, 1990]. The MATW model incorporates variations of both the bottom depth and the bottom density.

[31] The first attempt to explain the bottom flow in the EGC in Fram Strait as a result of a joint effect of the bottom slope and baroclinicity was made in the already mentioned study by *Schlichtholz and Houssais* [1999b]. The analytical model constructed in that study was based on a vorticity equation for the depth-averaged flow in which the so-called JEBAR (joint effect of baroclinicity and relief) term is balanced by a friction term. Instead of bottom density variations, the JEBAR term emphasizes along-isobath variations of potential energy per unit area, which depends on the density distribution from the bottom to the surface. If the friction term in that equation represents bottom friction, the equation becomes an equivalent of the vertically integrated vorticity equation (15) [e.g., *Mertz and Wright*, 1992]. However, analytical solutions obtained by *Schlichtholz and Houssais* [1999b] incorporated an assumption that the flow is uniform in the along-isobath direction. Certainly, this is only a rough approximation for the EGC between 80.5°N and 77.5°N (Figure 5). The present MATW model explains not only the existence of a bottom flow but accounts also for along-isobath variations of that flow.

6. Conclusion

[32] An assumption that the leading order vertically integrated vorticity balance in Fram Strait in summer is between the topographic vortex stretching and the bottom Ekman pumping has been substantiated using an inverse solution from SH. The balance has been then interpreted in terms of the MATW model which relates the bottom geostrophic flow to the bottom density. In particular, the along-isobath component of the flow should be driven by along-isobath variations of ρ_b. Such variations are present in the inverse solution as well as in the original MIZEX 84 data which has been shown for the EGC along the 2000 m isobath. In the EGC, ρ_b increases generally southward. A mean north-south density contrast along the 2000 m isobath in the strait is O(0.01 kg m^{-3}). It has been demonstrated that this contrast should be responsible for a bottom flow with a magnitude of O(3 cm s^{-1}). This estimate fits well the magnitude of the bottom flow from the inverse solution as well as from independent, direct current measurements at 79°N by *Foldvik et al.* [1988]. The validity of the MATW model in Fram Strait could have been suggested using only the density distribution from the MIZEX 84 data and the estimate of the magnitude of the near-bottom flow from the current measurements. The inverse solution indicates, in addition, that the along-isobath distributions of the along-isobath component of the bottom geostrophic flow and the bottom density are likely to be correlated. The correlation coefficient between v_b and ρ_b may be as large as -0.8.

[33] It was suggested in SH that the bottom flow in Fram Strait should be driven by along-isobath variations of potential energy per unit area. This inference was based on the analytical model of the EGC in Fram Strait presented in *Schlichtholz and Houssais* [1999b]. The MATW model is free of the assumption made in the latter study that the flow is uniform in the along-isobath direction. In any case, it is the baroclinicity in the presence of the bottom depth gradient which drives the bottom geostrophic flow in the EGC in summer. This interpretation was lacking in earlier concepts of exchange between the Arctic Ocean and the Nordic Seas through Fram Strait. One may wonder about the existence of a MATW in other parts of the Arctic Mediterranean. The West Spitsbergen Current and the deep EGC in Fram Strait are parts of the Arctic Circumpolar Boundary Current described qualitatively by *Rudels et al.* [1999]. Is this boundary current a MATW? If yes, what are the timescales of variability of this MATW? What is the role of wind forcing in that variability? These problems will be tackled in future studies.

[34] **Acknowledgments.** Academic Computer Center in Gdansk TASK is acknowledged for computational support. The author would like to thank the anonymous reviewers for their remarks.

References

Aagaard, K., Wind-driven transports in the Greenland and Norwegian Seas, *Deep Sea Res.*, *17*, 281–291, 1970.

Aagaard, K., C. Darnall, and P. Greisman, Year-long current measurements in the Greenland-Spitsbergen passage, *Deep Sea Res.*, *20*, 743–746, 1973.

Aagaard, K., J. H. Swift, and E. C. Carmack, Thermohaline circulation in the Arctic Mediterranean Seas, *J. Geophys. Res.*, *90*, 4833–4846, 1985.

Anderson, D. L. T., and R. A. Corry, Seasonal transport variations in the Florida Straits: A model study, *J. Phys. Oceanogr.*, *15*, 773–786, 1985.

Anderson, D. L. T., and D. Killworth, Spin-up of a stratified ocean, with topography, *Deep Sea Res.*, *24*, 709–732, 1977.

Colony, R., and A. Thorndike, An estimate of the mean field of ice motion, *J. Geophys. Res.*, *89*, 10,623–10,629, 1984.

Csanady, G. T., The arrested topographic wave, *J. Phys. Oceanogr.*, *8*, 47–62, 1978.

Foldvik, A., K. Aagaard, and T. Torresen, On the velocity field of the East Greenland Current, *Deep Sea Res. Part A*, *35*, 1335–1354, 1988.

Hunkins, K., A review of the physical oceanography of Fram Strait, in *The Physical Oceanography of Sea Straits*, edited by I. Pratt, pp. 61–93, Kluwer Acad., Norwell, Mass., 1990.

Hunkins, K., and J. A. Whitehead, Laboratory simulation of exchange through Fram Strait, *J. Geophys. Res.*, *97*, 11299–11321, 1992.

Jónsson, S., Seasonal and interannual variability of wind stress curl over the Nordic Seas, *J. Geophys. Res.*, *96*, 2649–2659, 1991.

Manley, T. O., K. L. Hunkins, and R. D. Muench, Current regimes across the East Greenland Polar Front at 78°40' north latitude during summer 1984, *J. Geophys. Res.*, *92*, 6741–6753, 1987.

Mertz, G., and D. G. Wright, Interpretations of the JEBAR term, *J. Phys. Oceanogr.*, *22*, 301–305, 1992.

Pedlosky, J., Ocean Circulation Theory, Springer-Verlag, New York, 1996.

Rudels, B., H. J. Friedrich, and D. Quadfasel, The Arctic Circumpolar Boundary Current, *Deep Sea Res. Part II*, *46*, 1023–1062, 1999.

Sakamoto, T., and T. Yamagata, Seasonal transport variations of the wind-driven ocean circulation in a two-layer planetary geostrophic model with a continental slope, *J. Mar. Res.*, *54*, 261–284, 1996.

Schlichtholz, P., and M.-N. Houssais, An inverse modeling study in Fram Strait, part I, Dynamics and circulation, *Deep Sea Res., Part II*, *46*, 1083–1135, 1999a.

Schlichtholz, P., and M.-N. Houssais, An investigation of the dynamics of the East Greenland Current in Fram Strait based on a simple analytical model, *J. Phys. Oceanogr.*, *29*, 2240–2265, 1999b.

Shaw, P.-T., and G. T. Csanady, Self-advection of density perturbations on a sloping continental shelf, *J. Phys. Oceanogr.*, *13*, 769–782, 1983.

Stigebrandt, A., A model for the thickness and salinity of the upper layer of the Arctic Ocean and the relationship between ice thickness and some external parameters, *J. Phys. Oceanogr.*, *11*, 1407–1422, 1981.

Wadhams, P., A. E. Gill, and P. F. Linden, Transects by submarine of the East Greenland Polar Front, *Deep Sea Res., Part A*, *26*, 1311–1327, 1979.

Wunsch, C., *The Ocean Circulation Inverse Problem*, Cambridge Univ. Press, New York, 1996.

P. Schlichtholz, Institute of Oceanology, Polish Academy of Sciences, Powstancow Warszawy 55, 81-712 Sopot, Poland. (schlicht@iopan.gda.pl)